



1 *Type of the Paper (Article)*

# 2 **Metal-free modified boron nitride for enhanced CO<sub>2</sub>** 3 **capture**

4 **Fereshteh Hojatisaeidi<sup>1</sup>, Mauro Mureddu<sup>2</sup>, Federica Dessì<sup>2</sup>, Geraldine Durand<sup>1,3</sup> and Basudeb**  
5 **Saha<sup>1</sup> \***

6 <sup>1</sup> School of Engineering, London South Bank University, 103 Borough Road, London SE1 0AA, United  
7 Kingdom

8 <sup>2</sup> Sotacarbo S.p.A. Grande Miniera di Serbariu, 09013 Carbonia (CA), Italy

9 <sup>3</sup> The Welding Institute, Granta Park, Great Abington, Cambridge, CB21 6AL, United Kingdom

10 \* Corresponding Author: School of Engineering, London South Bank University, 103 Borough Road, London  
11 SE1 0AA. Tel.: +44 (0)20 7815 7190; Fax: +44 (0)20 7815 7699. E-mail address: [b.saha@lsbu.ac.uk](mailto:b.saha@lsbu.ac.uk) (B. Saha).

12 **Abstract:** Porous boron nitride is a new class of solid adsorbent with applications in CO<sub>2</sub> capture. In  
13 order to further enhance the adsorption capacities of materials, new strategies such as porosity  
14 tuning, element doping and surface modification have been taken into account. In this work, metal-  
15 free modification of porous boron nitride (BN) has been prepared by a structure directing agent *via*  
16 simple heat treatment under N<sub>2</sub> flow. We have demonstrated that textural properties of BN play a  
17 pivotal role in CO<sub>2</sub> adsorption behavior. Therefore, addition of a triblock copolymer surfactant  
18 (P123) has been adopted to improve the pore ordering and textural properties of porous BN and its  
19 influence on the morphological and structural properties of pristine BN has been characterised. The  
20 obtained BN-P123 exhibits a high surface area of 476 m<sup>2</sup>/g, a large pore volume of 0.83 cm<sup>3</sup>/g with  
21 an abundance of micropores. More importantly, after modification with P123 copolymer, the  
22 capacity of pure CO<sub>2</sub> on porous BN has improved by about 34.5% compared to pristine BN (2.69  
23 mmol/g for BN-P123 *vs.* 2 mmol/g for pristine BN under ambient condition). The unique  
24 characteristics of boron nitride opens up new routes for designing porous BN, which could be  
25 employed for optimizing CO<sub>2</sub> adsorption.

26 **Keywords:** Porous boron nitride; metal-free modification; structure directing agent; CO<sub>2</sub> capture.  
27

## 28 **1. Introduction**

29 Over the last decades, climate change has become a global challenge for countries across the  
30 world [1]. Carbon capture and storage (CCS) is expected to play a substantial role in meeting the  
31 global warming targets set by the Inter-governmental Panel on Climate Change (IPCC) [2]. It is a  
32 promising option to maintain fossil fuels as a global central energy contributor and is expected to  
33 progress in lab scale, pilot scale, demonstration scale and commercial scale [3]. Chemical absorption  
34 technology, which has been used to remove CO<sub>2</sub> from natural gas, is reached to the commercial phase  
35 of development and several pilot-scale projects have been conducted since decades ago [4,5]. To date,  
36 the capture technologies that have been demonstrated in pilot plant scale or higher are classified as  
37 (i) post-combustion, (ii) pre-combustion, and (iii) oxy-fuel combustion [6]. Among the current  
38 available technologies, CO<sub>2</sub> capture from post-combustion emission gases is the most common  
39 technology in power plants and industries. Effective methods to separate, capture, store and convert  
40 CO<sub>2</sub> have attracted increasing attention [7]. The current technology for CO<sub>2</sub> capture is based on  
41 absorption in aqueous organic amines [8]. However, the intensive energy consumption, equipment  
42 corrosion and toxicity, make exploration of new materials for CO<sub>2</sub> capture highly demanding [9].

43 Solid adsorption is an alternative process to solvent-based chemisorption, which can be applied  
44 for a wide range of temperature and pressure conditions. Also, it can be designed for both post-  
45 combustion and pre-combustion applications. One of the challenges in this area relates to the  
46 manufacturing of new adsorbents that enables enhancing good diffusion kinetics and providing

47 improved performance [10]. In this regards, porous materials with high porosity, chemical and  
48 thermal stability are promising solid adsorbents for capturing CO<sub>2</sub> [11,12]. Among various kinds of  
49 porous materials, such as zeolites [13,14], porous polymers [15], metal-organic framework [16,17],  
50 activated carbons [18], porous BN has become one of the new classes of CO<sub>2</sub> adsorbents. Due to  
51 intrinsic properties of boron nitride such as high thermal and oxidation stability, large surface area  
52 and polarity, porous boron nitride is a desired alternative for CO<sub>2</sub> capture [19,20]. However,  
53 according to theoretical and experimental works, the interaction between pristine BN and CO<sub>2</sub> is very  
54 weak due to electron deficient nature of boron atoms and the Lewis acidic nature of CO<sub>2</sub> [21,22,23].  
55 To overcome such disadvantages, some strategies in view of tuning the structure, pore size and  
56 charge state of the BN have been studied. Nag et al. [24] made a few-layered BN by controlled  
57 chemical synthesis. Similarly, the effects of different proportions of urea on the number of BN layers  
58 indicate that the sample with the lowest layer thickness shows a high CO<sub>2</sub> uptake. Xiao et al. [25]  
59 reported a few layered porous boron nitride nanosheets (BNNs) by using magnesium diboride  
60 (MgB<sub>2</sub>) as a dynamic template. However, the CO<sub>2</sub> uptake of their work was relatively low (0.45  
61 mmol/g), while it demonstrated excellent selectivity of CO<sub>2</sub> over N<sub>2</sub>. Yang et al. [26] developed a three  
62 dimensional (3D) functionalized porous BN with flower-like morphology and high specific surface  
63 area ~1114 m<sup>2</sup>/g, and it shows 1.69 mmol/g CO<sub>2</sub> capture capacity at 1 bar and 273 K. It is also  
64 interesting to note that in most studies, element doping, and surface functionalization of boron nitride  
65 is critical to increase the CO<sub>2</sub> adsorption capacity. For instance, Chen et al. [27] produced ultrahigh  
66 microporous volume of boron carbon nitride (BCN) by doping carbon into hexagonal structure of  
67 BN. The performance of BCN material displays increased relative to pure BN for CO<sub>2</sub> uptake and  
68 reached up to 3.91 mmol/g at 298 K and ambient pressure. In addition, Huang et al. [28] enriched the  
69 interaction between electron-deficient boron atoms in BN and CO<sub>2</sub> molecules by aminopolymer-  
70 functionalized BN nanosheets. Therefore, porous structure and surface chemistry features of BN-  
71 based materials play crucial roles in CO<sub>2</sub> adsorption performance and it remains a challenge to control  
72 the parameters of boron nitride porosity and develop novel structures with high capacitive  
73 performance for carbon capture.

74 In this work, with the aim of achieving high CO<sub>2</sub> adsorption capacity of porous BN through  
75 tuning the porosity, BN structure has been modified in the presence of P123 as a structure directing  
76 agent. The synthesized BN-P123 possesses high specific surface area and pore volume compared to  
77 pristine BN, which results in an enhanced CO<sub>2</sub> adsorption capacity.

## 78 2. Materials and Methods

79 Metal-free modified BN was synthesized on a two-step method of solvent evaporation and high  
80 thermal decomposition [29]. Boric acid (ACS reagent, Sigma-Aldrich), urea (for synthesis, Sigma-  
81 Aldrich) and Pluronic P123 triblock copolymers (M<sub>n</sub> ~5800, Sigma-Aldrich) based on poly(ethylene  
82 glycol)-poly(propylene glycol)-poly(ethylene glycol) were used as raw materials. In detail, boric acid  
83 and urea with molar ratio 1:30 were added into 50 ml deionized water. Then 0.5 g P123 was  
84 introduced into the mixture solution and heated up at 338 K under vigorous stirring. A white  
85 precipitate was obtained after complete evaporation of water at that temperature. Afterwards, the  
86 precursor was dried into the oven for 24 hours and annealed at 1173 K under N<sub>2</sub> gas (the flow rate is  
87 150 ml/min) for 3 hours. Finally, modified porous BN was collected and marked as BN-P123. For  
88 comparison, pristine BN was also prepared following the same procedure without adding any  
89 surfactant.

90 The morphology of samples was collected scanning electron microscope (SEM, PEMTRON PS-  
91 230) in secondary electron mode (SE detector) at 10 kV. The microscope was equipped with an  
92 energy-dispersive X-ray (EDX, OXFORD X-act) with energy resolution at 5.9 keV for the local  
93 elemental analysis. The samples were ground, deposited on carbon tape, and coated (BIO-RAD  
94 sputter coater) with gold to reduce charging in the microscope.

95 X-ray diffraction (XRD) was performed to evaluate the structural properties using an X-ray  
96 diffractometer (Bruker D8 Advance) in reflection mode. The diffraction patterns run at an anode  
97 voltage of 40 kV and an emission current of 40 mA using monochromatic Cu K $\alpha$  radiation ( $\lambda$ = 1.541  
98 78 Å). The intermolecular bonding and chemical properties of the materials were characterized by  
99 Fourier-transform infrared (FTIR) spectroscopy. The spectra were recorded on a Nicolet Avatar 370

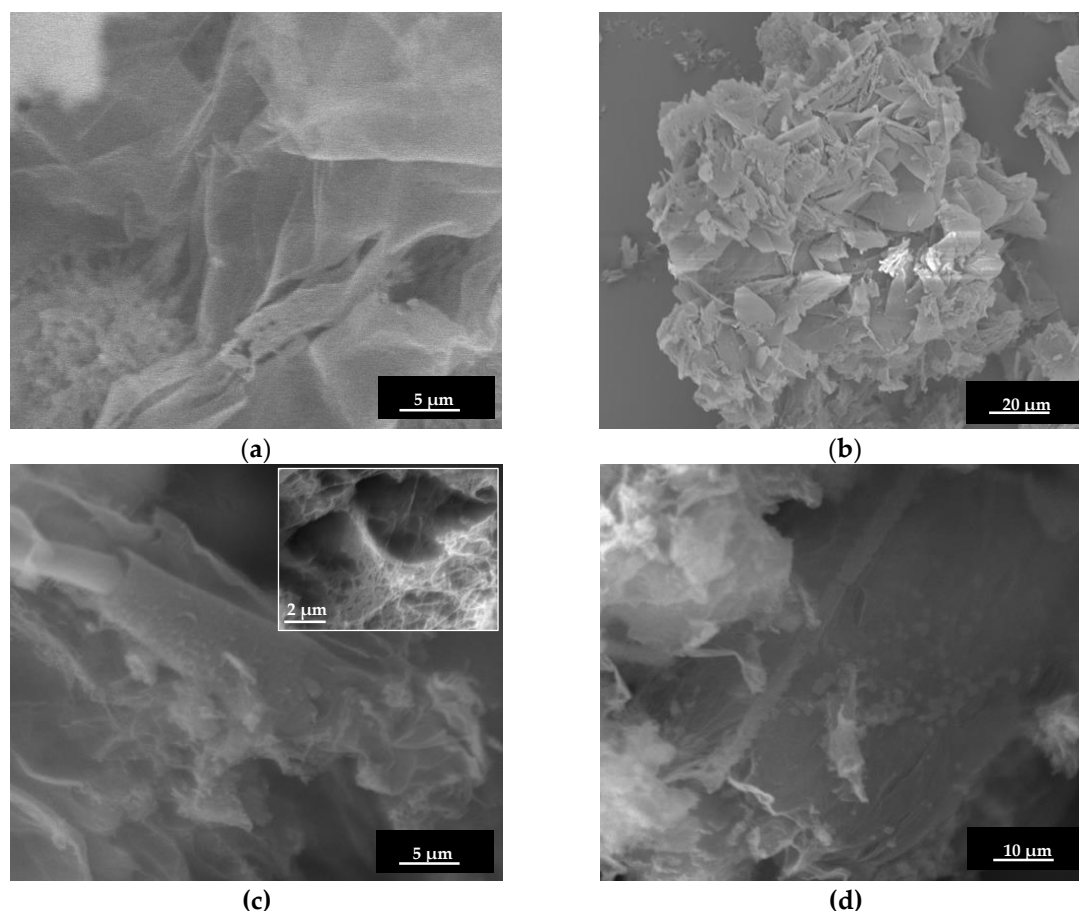
100 spectrometer from 4000 to 400  $\text{cm}^{-1}$  using KBr pellets at room temperature. Optical absorption  
101 measurement (SHIMADZU UV-1800) was measured. Prior to the measurement, the powder  
102 materials were dispersed in water (50 mg of samples in 25 ml water at room temperature). The  
103 thermal stability of samples was performed using thermal gravimetric analysis (TGA), Ultra micro  
104 balance, Mettler Toledo. An alumina pan was loaded with 5-10 mg of sample material and heated  
105 from room temperature to 1273 K at a rate of 10 K/ min in air atmosphere.

106 Nitrogen isotherms were obtained using a porosity analyzer (Micromeritics ASAP2060) at 77 K.  
107 The surface areas of the samples were calculated using the Brunauer–Emmett–Teller (BET) method.  
108 The total volume of pores was calculated using the software from the BJH adsorption calculation.  
109 The  $\text{CO}_2$  adsorption and desorption performance were evaluated with a TGA/DSC 3+ micro balance,  
110 Mettler Toledo. The  $\text{CO}_2$  capture capacity of the sorbents were determined by measuring the mass  
111 uptake of the sample during the  $\text{CO}_2$  adsorption.

### 112 3. Results and discussion

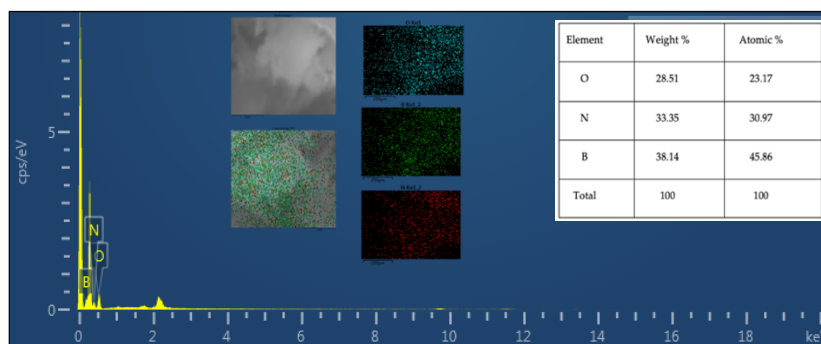
#### 113 3.1. Sample characterisation

114 The morphology of samples was studied using scanning electron microscopy (SEM). The  
115 pristine BN exhibited an ultrathin flake-like morphology, as displayed in (Figures 1a–b). BN-P123  
116 presented a cloud-like sheet structure with interconnected network of porous structure (Figures 1c–  
117 d). Moreover, the formation of pristine BN and BN-P123 were studied by EDX and elemental  
118 mapping (Figures 2a–b). It is obvious that the product is mainly comprised of boron (B), nitrogen (N)  
119 and oxygen (O). As shown in Figure 2b, BN-P123 has very little increase in oxygen content compared  
120 to pristine BN. This is due to the introduction of P123 into BN formation.  
121

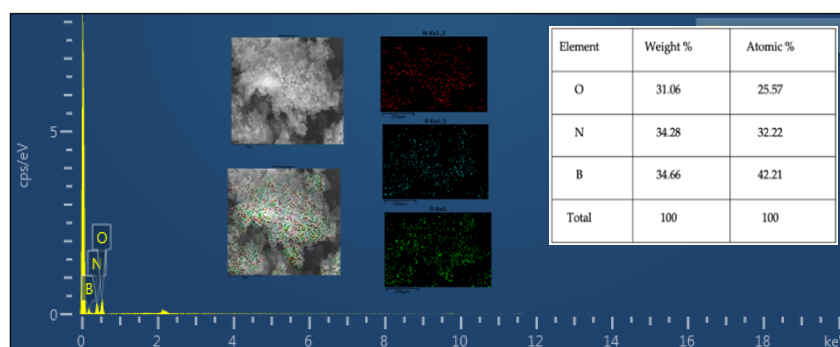


122 **Figure 1.** SEM images of (a, b) pristine BN; (b, c) BN-P123. The insert shows the interconnected porous  
123 structure.

124



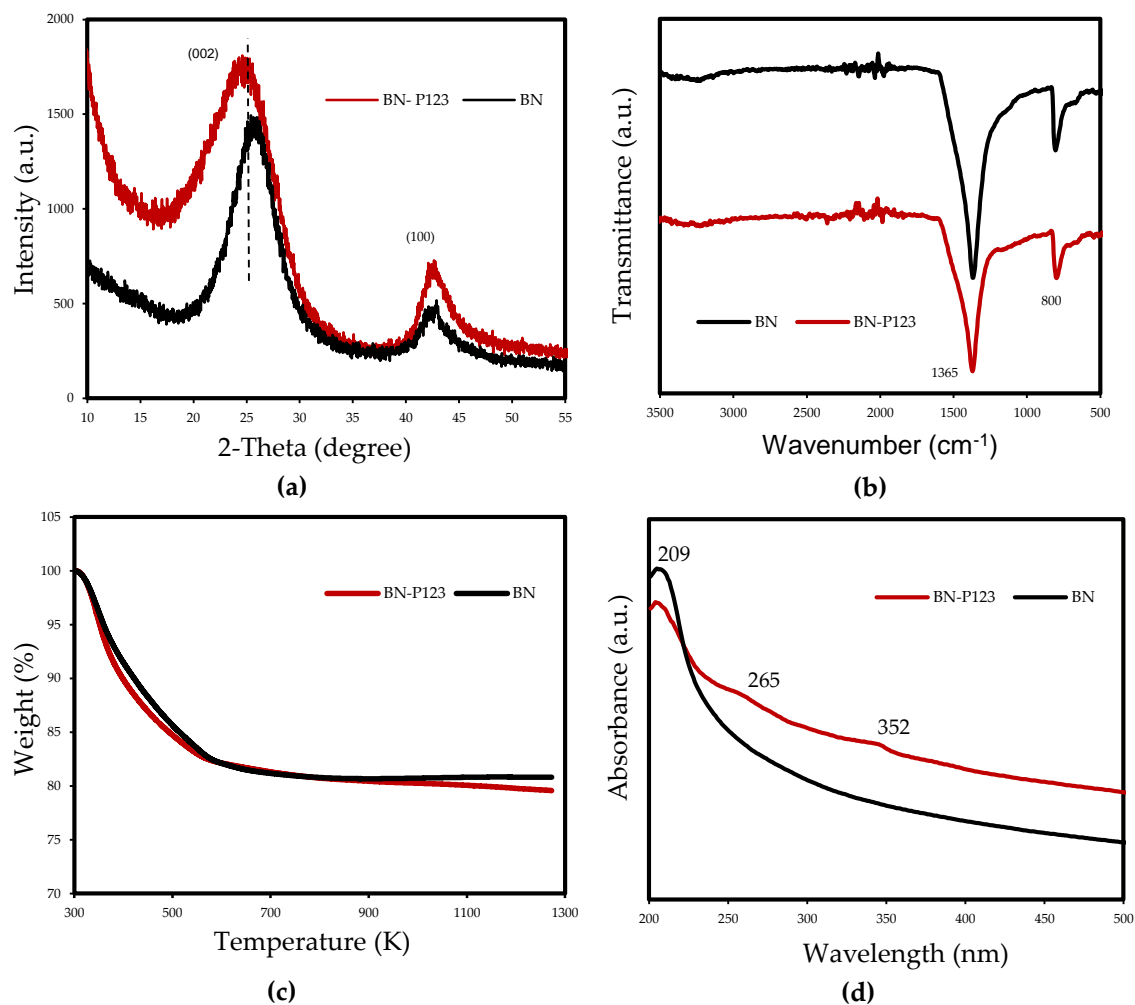
(a)



(b)

125 **Figure 2.** EDX spectra of (a) pristine BN; (b) BN-P123 and the insert show the elemental mapping and  
 126 corresponding atomic % of elements.

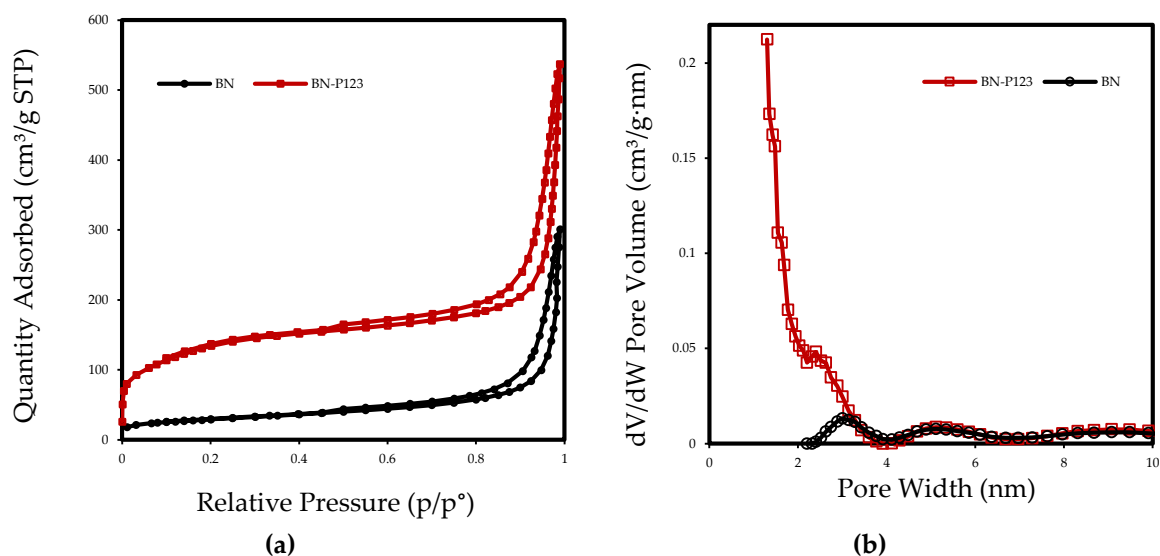
127 The structure of samples was analysed and Figure 3a depicts the XRD patterns of the prepared  
 128 samples. The results show two characteristic peaks around  $\sim 25^\circ$  and  $\sim 42^\circ$  which are attributed to  
 129 the (002) and (100) crystal planes of hexagonal boron nitride, respectively [30]. Additionally, the  
 130 peaks of both samples confirmed the poor crystallization with the presence of turbostratic material.  
 131 Compared with pristine BN, the (002) diffraction peaks of BN-P123 shifted to a lower angle, which  
 132 promote more disordered hexagonal boron nitride (h-BN) structure. More details of the chemical  
 133 features were supported by Fourier transform infrared (FT-IR) spectroscopy and the results are  
 134 shown in Figure 3b. All peaks exhibited two main characteristic bands of boron nitride at  $\sim 1365$  and  
 135  $800\text{ cm}^{-1}$  corresponding to in-plane B-N transverse optical mode and out-of-plane B-N-B bending  
 136 mode, respectively [31]. No major chemical differences could be observed between the samples.  
 137 Thermal stability of samples was performed in air atmosphere (rate=10 K/min) and shown in Figure  
 138 3c. The TG thermograms reflected the weight loss of 19% for both samples, representing the removal  
 139 of moisture adsorbed on the material surface. After 573 K the lines show the thermal stability nature  
 140 of BN at high temperature and there was no significant weight loss up to 1273 K. The UV-vis  
 141 absorption collected in Figure 3d indicates a highly transparent from visible to UV wavelength [32].  
 142 The maximum absorption peak around 209 nm, is attributed to intrinsic excitation absorption band  
 143 of h-BN. Besides, small humps around 265 and 352 nm were detected in BN-P123, corresponding to  
 144 impurities. So far, above all characteristic results on both samples, it was found that the structure and  
 145 chemical nature of BN has not changed after modifying BN with the surfactant compound and both  
 146 samples revealed almost similar features. We assumed that the utilisation of block copolymer (P123)  
 147 might affect the textural properties of pristine BN.  
 148



149 **Figure 3.** XRD patterns (a); FT-IR (b); TGA curves of prepared samples (c) and UV-Vis (d).

### 150 3.2. Textural Analysis

151 The textural properties of pristine BN and BN-P123 adsorbent were obtained by nitrogen  
 152 adsorption/desorption isotherm at 77 K and the results are summarized in Table 1. As indicated in  
 153 Figure 4a, the resulting isotherms display a typical type II curve based on IUPAC classification and  
 154 type H3 hysteresis loop in the partial pressure range 0.4-1.0, which indicates the presence of mesopores  
 155 and slit shape pores [33]. There is a trivial rise in N<sub>2</sub> adsorption-desorption isotherm of BN-P123 at  
 156 lower pressure ( $P/P_0 < 0.25$ ), which is caused by presence of micropores [34]. The non-local density  
 157 functional theory (NLDFT) was used to calculate pore size distributions. As expected, the  $dV/dW$  pore  
 158 volume of BN-P123 increases dramatically with abundance of micropores (Figure 4b). Meanwhile,  
 159 using the Brunauer–Emmett–Teller (BET) method [35], the specific surface areas are calculated  
 160 showing that the BET surface area of BN-P123 is much higher than pristine BN (Table 1). It is clear  
 161 from the above measurements that the P123 introduced into precursors during the fabrication process  
 162 is highly effective on the microscale structure of porous BN and improves surface area and pore  
 163 volume of the sample.



164 **Figure 4.** Nitrogen adsorption-desorption isotherm of the pristine BN and BN-P123 (a); NLDFT pore size  
 165 distribution curves of the same samples (b).

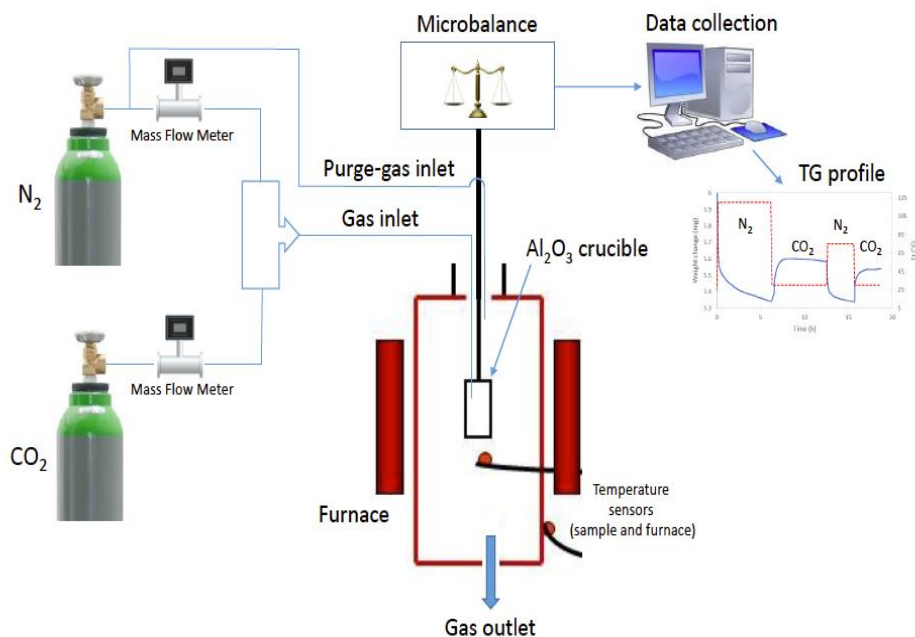
166 Table 1. Textural properties and CO<sub>2</sub> capacity (298 K) of prepared materials.

sample	$S_{\text{BET}}^1$ (m <sup>2</sup> /g)	$V_{\text{total}}^2$ (cm <sup>3</sup> /g)	CO <sub>2</sub> Uptake (mmol/g)
Pristine BN	102	0.46	2.00
BN-P123	476	0.83	2.69

167 <sup>1</sup> Specific surface area (m<sup>2</sup>/g) obtained by Brunauer-Emmett-Teller (BET) method. <sup>2</sup> Total pore volume (cm<sup>3</sup>/g)  
 168 calculated at  $P/P_0 = 0.99$ .

### 169 3.3. Gas adsorption analysis

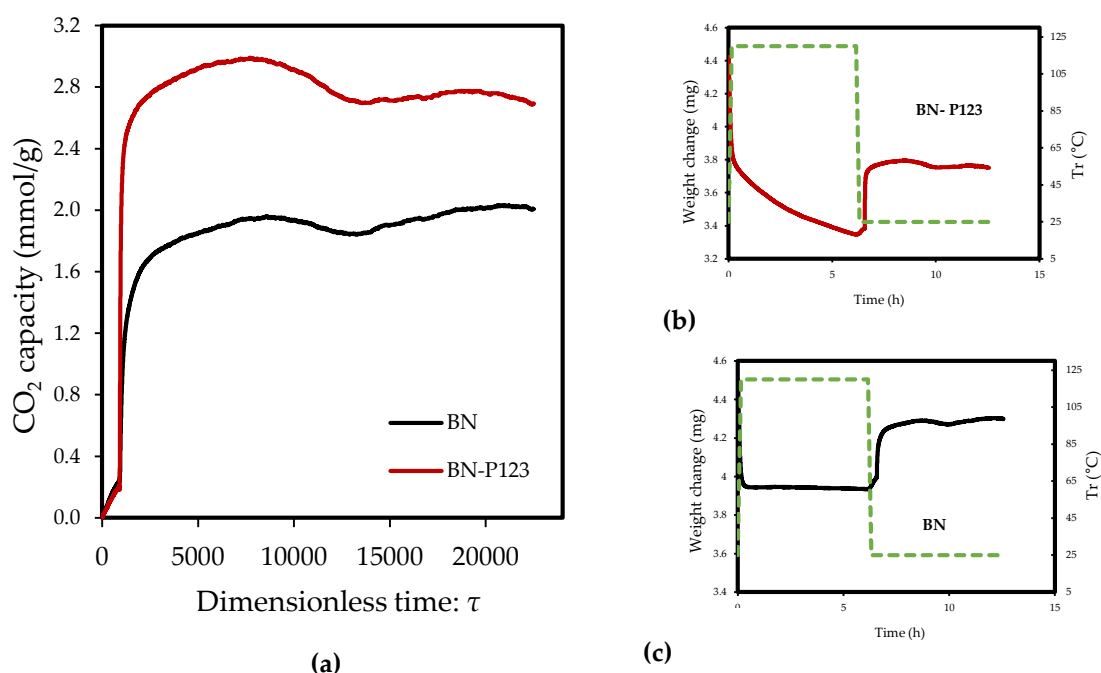
170 Due to the relatively large porosity of samples, the modified sample BN-P123 and pristine BN  
 171 were assessed for CO<sub>2</sub> capture under ambient conditions. The adsorption capacities of pure CO<sub>2</sub> on  
 172 pristine BN and BN-P123 were determined by thermogravimetric analysis. Prior to the sorption test,  
 173 samples were dried at 393 K with a heating rate of 10 K/min from 298 K under flowing N<sub>2</sub> (150  
 174 ml/min) for 6 hours and then allowed to cool to the temperature at which the sorption is carried out  
 175 at 298 K with a heating rate of 10 K/min. When the sorption temperature was reached, samples were  
 176 stabilized under flowing N<sub>2</sub> (99,999%, 150 ml/min) for 15 min and then N<sub>2</sub> flow was switched to pure  
 177 CO<sub>2</sub> (99,999%, 50 ml/min) flow for 6 hours. The mass uptake during this stage was interpreted as the  
 178 CO<sub>2</sub> capture capacity. Figures 5 and 6 (a-c) illustrate the setup of experiments and the TG profiles of  
 179 CO<sub>2</sub> uptake along with weight change results respectively.



180

181

**Figure 5.** Illustration of CO<sub>2</sub> adsorption experiment.



182

**Figure 6.** TG profiles of CO<sub>2</sub> adsorption on Pristine BN and BN- P123 (a); TG profiles of weight change on the same samples (b,c).

183

184

The experiments reveal that pristine BN shows a CO<sub>2</sub> capacity of 2 mmol/g at 298 K, which enhanced with the addition of P123 copolymer (2.69 mmol/g for BN-P123 at 298 K) (Table 1). The augmented CO<sub>2</sub> adsorption on BN-P123 sample is undoubtedly as a result of the porous morphology of modified BN, whereas pristine BN exhibits lower porosity. It is well-known that higher microporosity provides more active sites and storage space to boost the adsorption performances [36,37,38]. To the best of our knowledge, the result of our synthetic method is higher than other modification methods such as (3D) BCNO structure (1.8 mmol/g) at 298 K as reported by Lopez-Salas et al. [39] and closer to porous BCN (2.49 mmol/g) at 298 K and porous BN fiber (2.85 mmol/g) at 273 K [40,41]. However, the use of melamine in porous BCN as well as BN fiber leads to the presence of

189

190

191

192

193 carbon content and consequently decreases the stability upon exposure to ambient air. The effect of  
 194 high-temperature treatment in different gases was studied in [42], where porous BN fibers treated in  
 195  $\text{NH}_3$  gas at 1673–1773 K enhanced  $\text{CO}_2$  adsorption capacity (from 0.45 mmol/g to 1.6 mmol/g).  
 196 Nonetheless, this outcome is not a satisfactory result. One possible insight of this finding is that  
 197 pyrolysis temperature and carrier gas does not lead to a remarkable change in  $\text{CO}_2$  uptake. In  
 198 addition, directing triblock co-polymer was also used to design a hierarchical carbon sorbent [43].  
 199 This hierarchical structure is desirable for  $\text{CO}_2$  capture as it shows superior capacity (4.5 mmol/g)  
 200 under ambient conditions. It is noteworthy that at lower pressures ( $\text{bar} \leq 1$ ), the density of pore  
 201 volume, especially the micropores volume plays a critical role in capturing  $\text{CO}_2$  [44]. Therefore, high  
 202 surface area and porosity of BN-P123 has brought about a positive adsorption interaction.

203 It is to be noted that for the pristine BN (without adding surfactant) the  $\text{CO}_2$  adsorption capacity  
 204 on our sample exceeds those materials reported by Marchesini et al. [45,46]. Although they  
 205 accomplished highly porous boron nitride with a high surface area ( $>1900 \text{ m}^2/\text{g}$ ), the  $\text{CO}_2$  adsorption  
 206 capacity of their sample was up to 1.6 mmol/g under ambient condition. Given the results of our  
 207 approach, one can conclude that though the specific surface area (SSA) is one of the main factors to  
 208 increase the  $\text{CO}_2$  capacity, obtaining a high SSA e.g. ( $>1000 \text{ m}^2/\text{g}$ ) does not lend itself to an increased  
 209  $\text{CO}_2$  capacity.  
 210

## 211 5. Conclusions

212 In summary, the porosity of boron nitride has been successfully tuned by introducing the  
 213 triblock copolymer surfactant (P123) during the preparation process of BN precursors. In particular,  
 214 we found that by utilizing the P123 into boron and nitrogen precursors leads to improved  $\text{CO}_2$   
 215 adsorption capacity up to 2.69 mmol/g, as compared with pristine porous BN which was found 2.00  
 216 mmol/g. Furthermore, based on the structural properties and morphology results obtained in this  
 217 work, we determine that both samples share almost similar chemical features. However, the porosity  
 218 of samples revealed a remarkable change and for the sample BN-P123 ( $0.83 \text{ cm}^3/\text{g}$ ), it was virtually  
 219 quadrupled as a result of the modification. This significant change is attributed to the formation of  
 220 more gases during the decomposition process, thereby creating higher porosity levels. A natural  
 221 progression of this work is to describe how textural property parameters of BN lead to higher  
 222 interaction between BN and  $\text{CO}_2$  molecules. Our work could be extended by exploring other  
 223 parameters (e.g. electronic features or surface chemistry of BN), which could influence on BN to  
 224 capture more  $\text{CO}_2$ . All in all, our analyses demonstrate the applicability of metal-free modification of  
 225 BN for enhanced capacity of pure  $\text{CO}_2$ .

226 **Funding:** F.H. was partially funded by School of Engineering, London South Bank University.

227 **Acknowledgments:** The Sotacarbo contribution in this work has been carried out within the “Centre of  
 228 Excellence on Clean Energy” project (CUP: D83C17000370002), funded by the Regional Government of Sardinia  
 229 (FSC 2014-2020).

230 **Conflicts of Interest:** The authors declare no conflict of interest.

## 231 References

- 232 1. Oschatz, M.; Antonietti, M. A search for selectivity to enable  $\text{CO}_2$  capture with porous adsorbents.  
 233 *Energy Environ. Sci.* **2018**, *11*, 57–70.
- 234 2. Strielkowski, W.; Lisin, E.; Gryshova, I. Climate policy of the European Union: what to expect from the  
 235 Paris agreement. *Rom. J. Eur. Aff.* **2016**, *16*, 68.
- 236 3. Bui, M.; Adjiman, C.S.; Bardow, A.; Anthony, E.J.; Boston, A.; Brown, S.; Fennell, P.S.; Fuss, S.; Galindo,  
 237 A.; Hackett, L.A. Carbon capture and storage (CCS): the way forward. *Energy Environ. Sci.* **2018**.
- 238 4. Akinpelumi, K.; Saha, C.; Rochelle, G.T. Piperazine aerosol mitigation for post-combustion carbon  
 239 capture. *Int. J. Greenh. Gas Control* **2019**.
- 240 5. Mantripragada, H.C.; Zhai, H.; Rubin, E.S. Boundary Dam or Petra Nova – Which is a better model for



- 241 CCS energy supply? *Int. J. Greenh. Gas Control* **2019**.
- 242 6. Lee, S.-Y.; Park, S.-J. A review on solid adsorbents for carbon dioxide capture. *J. Ind. Eng. Chem.* **2015**, *23*,  
243 1–11.
- 244 7. Yang, H.; Xu, Z.; Fan, M.; Gupta, R.; Slimane, R.B.; Bland, A.E.; Wright, I. Progress in carbon dioxide  
245 separation and capture: A review. *J. Environ. Sci.* **2008**, *20*, 14–27.
- 246 8. Li, B.; Duan, Y.; Luebke, D.; Morreale, B. Advances in CO<sub>2</sub> capture technology: A patent review. *Appl.*  
247 *Energy* **2013**, *102*, 1439–1447.
- 248 9. Férey, G.; Serre, C.; Devic, T.; Maurin, G.; Jobic, H.; Llewellyn, P.L.; De Weireld, G.; Vimont, A.; Daturi,  
249 M.; Chang, J.-S. Why hybrid porous solids capture greenhouse gases? *Chem. Soc. Rev.* **2011**, *40*, 550–562.
- 250 10. Wang, J.; Huang, L.; Yang, R.; Zhang, Z.; Wu, J.; Gao, Y.; Wang, Q.; O'Hare, D.; Zhong, Z. Recent  
251 advances in solid sorbents for CO<sub>2</sub> capture and new development trends. *Energy Environ. Sci.* **2014**, *7*,  
252 3478–3518.
- 253 11. Gargiulo, N.; Pepe, F.; Caputo, D. CO<sub>2</sub> adsorption by functionalized nanoporous materials: a review. *J.*  
254 *Nanosci. Nanotechnol.* **2014**, *14*, 1811–1822.
- 255 12. Pardakhti, M.; Jafari, T.; Tobin, Z.; Dutta, B.; Moharreri, E.; Saveh Shemshaki, N.; Suib, S.L.; Srivastava,  
256 R. Trends in solid adsorbent materials development for CO<sub>2</sub> capture. *ACS Appl. Mater. Interfaces* **2019**.
- 257 13. Yang, S.; Zhan, L.; Xu, X.; Wang, Y.; Ling, L.; Feng, X. Graphene-based porous silica sheets impregnated  
258 with polyethyleneimine for superior CO<sub>2</sub> capture. *Adv. Mater.* **2013**, *25*, 2130–2134.
- 259 14. Mendes, P.A.P.; Ribeiro, A.M.; Gleichmann, K.; Ferreira, A.F.P.; Rodrigues, A.E. Separation of CO<sub>2</sub>/N<sub>2</sub>  
260 on binderless 5A zeolite. *J. CO<sub>2</sub> Util.* **2017**.
- 261 15. Irani, M.; Jacobson, A.T.; Gasem, K.A.M.; Fan, M. Facilely synthesized porous polymer as support of  
262 poly(ethyleneimine) for effective CO<sub>2</sub> capture. *Energy* **2018**, *157*, 1–9.
- 263 16. Zhang, J. Design and synthesis of metal organic frameworks for co<sub>2</sub> separation and catalysis 2013.
- 264 17. Cota, I.; Martinez, F.F. Recent advances in the synthesis and applications of metal organic frameworks  
265 doped with ionic liquids for CO<sub>2</sub> adsorption. *Coord. Chem. Rev.* **2017**.
- 266 18. Ello, A.S.; de Souza, L.K.C.; Trokourey, A.; Jaroniec, M. Coconut shell-based microporous carbons for  
267 CO<sub>2</sub> capture. *Microporous Mesoporous Mater.* **2013**, *180*, 280–283.
- 268 19. Weng, Q.; Wang, X.; Wang, X.; Bando, Y.; Golberg, D. Functionalized hexagonal boron nitride  
269 nanomaterials: emerging properties and applications. *Chem. Soc. Rev.* **2016**, *45*, 3989–4012.
- 270 20. Shtansky, D. V.; Firestein, K.L.; Golberg, D. V. Fabrication and application of BN nanoparticles,  
271 nanosheets and their nanohybrids. *Nanoscale* **2018**, *10*, 17477–17493.
- 272 21. Sun, Q.; Li, Z.; Searles, D.J.; Chen, Y.; Lu, G.; Du, A. Charge-controlled switchable CO<sub>2</sub> capture on boron  
273 nitride nanomaterials. *J. Am. Chem. Soc.* **2013**, *135*, 8246–8253.
- 274 22. Choi, H.; Park, Y.C.; Kim, Y.-H.; Lee, Y.S. Ambient carbon dioxide capture by boron-rich boron nitride  
275 nanotube. *J. Am. Chem. Soc.* **2011**, *133*, 2084–2087.
- 276 23. Owuor, P.S.; Park, O.-K.; Woellner, C.F.; Jalilov, A.S.; Susarla, S.; Joyner, J.; Ozden, S.; Duy, L.; Villegas  
277 Salvatierra, R.; Vajtai, R. Lightweight hexagonal boron nitride foam for co<sub>2</sub> absorption. *ACS Nano* **2017**,  
278 *11*, 8944–8952.
- 279 24. Nag, A.; Raidongia, K.; Hembram, K.P.S.S.; Datta, R.; Waghmare, U. V.; Rao, C.N.R. Graphene analogues  
280 of BN: novel synthesis and properties. *ACS Nano* **2010**, *4*, 1539–1544.
- 281 25. Xiao, F.; Chen, Z.; Casillas, G.; Richardson, C.; Li, H.; Huang, Z. Controllable synthesis of few-layered  
282 and hierarchically porous boron nitride nanosheets. *Chem. Commun.* **2016**, *52*, 3911–3914.
- 283 26. Chen, Y.; Wang, J.; Chen, Y.; Liu, D.; Huang, S.; Lei, W. One-step template-free synthesis of 3D

- 284 functionalized flower-like boron nitride nanosheets for NH<sub>3</sub> and CO<sub>2</sub> adsorption. *Nanoscale* **2018**.
- 285 27. Chen, S.; Li, P.; Xu, S.; Pan, X.; Fu, Q.; Bao, X. Carbon doping of hexagonal boron nitride porous materials  
286 toward CO<sub>2</sub> capture. *J. Mater. Chem. A* **2018**.
- 287 28. Huang, K.; Liang, L.; Chai, S.; Tumuluri, U.; Li, M.; Wu, Z.; Sumpter, B.G.; Dai, S. Aminopolymer  
288 functionalization of boron nitride nanosheets for highly efficient capture of carbon dioxide. *J. Mater.*  
289 *Chem. A* **2017**, *5*, 16241–16248.
- 290 29. Xiong, J.; Yang, L.; Chao, Y.; Pang, J.; Zhang, M.; Zhu, W.; Li, H. Boron nitride mesoporous nanowires  
291 with doped oxygen atoms for the remarkable adsorption desulfurization performance from fuels. *ACS*  
292 *Sustain. Chem. Eng.* **2016**.
- 293 30. Kurakevych, O.O.; Solozhenko, V.L. Rhombohedral boron subnitride, B<sub>13</sub>N<sub>2</sub>, by X-ray powder  
294 diffraction. *Acta Crystallogr. Sect. C Cryst. Struct. Commun.* **2007**, *63*, i80–i82.
- 295 31. Liu, F.; Yu, J.; Ji, X.; Qian, M. Nanosheet-structured boron nitride spheres with a versatile adsorption  
296 capacity for water cleaning. *ACS Appl. Mater. Interfaces* **2015**, *7*, 1824–1832.
- 297 32. Ba, K.; Jiang, W.; Cheng, J.; Bao, J.; Xuan, N.; Sun, Y.; Liu, B.; Xie, A.; Wu, S.; Sun, Z. Chemical and  
298 bandgap engineering in monolayer hexagonal boron nitride. *Sci. Rep.* **2017**, *7*, 45584.
- 299 33. Pang, J.; Chao, Y.; Chang, H.; Li, H.; Xiong, J.; Zhang, Q.; Chen, G.; Qian, J.; Zhu, W.; Li, H. Silver  
300 nanoparticle-decorated boron nitride with tunable electronic properties for enhancement of adsorption  
301 performance. *ACS Sustain. Chem. Eng.* **2018**, *6*, 4948–4957.
- 302 34. Bi, W.; Hu, Y.; Li, W.; Jiang, H.; Li, C. Construction of nanoreactors combining two-dimensional  
303 hexagonal boron nitride (h-BN) coating with Pt/Al<sub>2</sub>O<sub>3</sub> catalyst toward efficient catalysis for CO  
304 oxidation. *Ind. Eng. Chem. Res.* **2018**, *57*, 13353–13361.
- 305 35. Brunauer, S.; Emmett, P.H.; Teller, E. Adsorption of gases in multimolecular layers. *J. Am. Chem. Soc.*  
306 **1938**, *60*, 309–319.
- 307 36. Li, J.; Xiao, X.; Xu, X.; Lin, J.; Huang, Y.; Xue, Y.; Jin, P.; Zou, J.; Tang, C. Activated boron nitride as an  
308 effective adsorbent for metal ions and organic pollutants. *Sci. Rep.* **2013**, *3*, 3208.
- 309 37. Xiong, J.; Li, H.; Yang, L.; Luo, J.; Chao, Y.; Pang, J.; Zhu, W. Metal-free boron nitride adsorbent for ultra-  
310 deep desulfurization. *AIChE J.* **2017**, *63*, 3463–3469.
- 311 38. Liu, F.; Li, S.; Yu, D.; Su, Y.; Shao, N.; Zhang, Z. Template-free synthesis of oxygen-doped bundlelike  
312 porous boron nitride for highly efficient removal of heavy metals from wastewater. *ACS Sustain. Chem.*  
313 *Eng.* **2018**, *6*, 16011–16020.
- 314 39. López-Salas, N.; Ferrer, M.L.; Gutiérrez, M.C.; Fierro, J.L.G.; Cuadrado-Collados, C.; Gandara-Loe, J.;  
315 Silvestre-Albero, J.; del Monte, F. Hydrogen-bond supramolecular hydrogels as efficient precursors in  
316 the preparation of freestanding 3D carbonaceous architectures containing BCNO nanocrystals and  
317 exhibiting a high CO<sub>2</sub>/CH<sub>4</sub> adsorption ratio. *Carbon N. Y.* **2018**, *134*, 470–479.
- 318 40. Florent, M.; Bandosz, T.J. Irreversible water mediated transformation of BCN from a 3D highly porous  
319 form to its nonporous hydrolyzed counterpart. *J. Mater. Chem. A* **2018**, *6*, 3510–3521.
- 320 41. Wang, D.; Xue, Y.; Wang, C.; Ji, J.; Zhou, Z.; Tang, C. Improved capture of carbon dioxide and methane  
321 via adding micropores within porous boron nitride fibers. *J. Mater. Sci.* **2019**, *54*, 10168–10178.
- 322 42. Liang, J.; Song, Q.; Lin, J.; Huang, Y.; Fang, Y.; Yu, C.; Xue, Y.; Liu, Z.; Tang, C. Pore structure regulation  
323 and carbon dioxide adsorption capacity improvement on porous BN fibers: Effects of high-temperature  
324 treatments in gaseous ambient. *Chem. Eng. J.* **2019**, *373*, 616–623.
- 325 43. To, J.W.F.; He, J.; Mei, J.; Haghpanah, R.; Chen, Z.; Kurosawa, T.; Chen, S.; Bae, W.-G.; Pan, L.; Tok, J.B.-  
326 H. Hierarchical N-doped carbon as CO<sub>2</sub> adsorbent with high CO<sub>2</sub> selectivity from rationally designed

- 327 polypyrrole precursor. *J. Am. Chem. Soc.* **2016**, *138*, 1001–1009.
- 328 44. Li, Y.; Ben, T.; Zhang, B.; Fu, Y.; Qiu, S. Ultrahigh gas storage both at low and high pressures in KOH-
- 329 activated carbonized porous aromatic frameworks. *Sci. Rep.* **2013**, *3*, 2420.
- 330 45. Marchesini, S.; Regoutz, A.; Payne, D.; Petit, C. Tunable porous boron nitride: Investigating its formation
- 331 and its application for gas adsorption. *Microporous Mesoporous Mater.* **2017**, *243*, 154–163.
- 332 46. Marchesini, S.; McGilvery, C.M.; Bailey, J.; Petit, C. Template-free synthesis of highly porous boron
- 333 nitride: insights into pore network design and impact on gas sorption. *ACS Nano* **2017**, *11*, 10003–10011.
- 334



© 2019 by the authors. Submitted for possible open access publication under the terms and conditions of the Creative Commons Attribution (CC BY) license (<http://creativecommons.org/licenses/by/4.0/>).

335